ADVANCED OPTICAL MATERIALS
www.advopticalmat.de

Single-Crystal Pd and its Alloy Nanowires for Plasmon Propagation and Highly Sensitive Hydrogen Detection

Fuxing Gu, Heping Zeng, Y. B. Zhu, Qing Yang, L. K. Ang, and Songlin Zhuang*

In this work plasmon propagation and highly sensitive hydrogen sensing are demonstrated in single-crystal Pd and its alloy nanowires, based on an evanescent wave coupling technique using optical fiber tapers. The plasmon propagation losses of Pd nanowires on an MgF_2 substrate are measured to be ~2 dB/μm (at 635 nm). Using a suspension scheme of the nanowire, the propagation losses decrease to ~0.6 dB/μm in air. Utilizing an alloying technique, single-crystal PdAg nanowires are fabricated and exhibit decreasing and tunable propagation losses. Furthermore, Pd nanowires are used for plasmonic gas sensing with amplitude sensitivity of ~11 dB to 3.6% hydrogen gas, which is much higher than those in photonic nanowire sensors. The concentration detection limit is about 0.2%, which is lower than those in photonic nanowire sensors and most surface plasmon resonance sensors. The hysteresis effect of the Pd nanowire in hydrogen sensing is suppressed by using single-crystal PdAu alloy nanowires. This work may find widespread application, ranging from sensing and integrated circuits to materials research.

1. Introduction

Because of the highly selective and reversible absorption of hydrogen within its crystal lattice and forming a palladium hydride phase, palladium (Pd) and its alloys such as Pd–Pt and Pd–Au have been well developed for hydrogen sensing applications.[1–4] One-dimensional Pd and its alloy nanostructures, such as nanocages,[5] nanodisks,[6] nanorods,[7] and nanowires,[8,9] have been attracting considerable attention due to the short diffusion lengths, which may differ from bulk materials both in their thermodynamic and phase transitions.[10,11] Understanding the physical principles behind the influence of nano-sizing on the Pd–H system and exploring novel sensing technique are therefore a key issue for developing efficient and robust Pd nanostructure-based hydrogen sensing devices.

Due to the tight field confinement beyond the diffraction limit in the visible and infrared region, surface plasmons has been a focus of intensive research activity in novel sensing techniques in recent years.[12–14] To date, surface plasmons of Pd nanostructures have been widely investigated in nanoparticle structures using localized surface plasmon resonance method,[5,6,10,11,15] which is typically excited via free space lasers.[16] In the irradiation configuration due to the nanoscale dimensions of the nanowire diameter and the relative large irradiation size, only a small portion of irradiated light can be intercepted by the nanowire, inducing low efficiency of the photon-to-plasmon conversion. In addition, using bulky components such as prisms or objectives are often required to excite surface plasmons, making it difficult to realize nanophotonic devices with miniaturized sizes and low power consumption.[17,18]

Compared with the methods that rely on free-space light focusing, guiding light along the entire nanowire waveguide could significantly enhance the light–nanowire interaction, which exhibits attractive advantages such as enhanced sensitivity,[17,19] reduced excitation power operation,[20,21] and tailorable waveguide dispersion.[22] Benefitted from the tightly confined local field, it is expected that developing surface plasmon propagation in Pd single nanowires may open new opportunities to hydrogen sensing with high sensitivity and low power operation.

Recently, single-crystal Pd nanowires synthesized via thermal evaporation method,[23,24] show promising candidates for low loss plasmonic waveguides, because of high crystallinity, atomic-scale surface smoothness, and good radial uniformity. These properties can reduce the propagation losses as compared with those metal waveguides fabricated by microfabrication techniques such as electrodeposition.[8,9] However, to our knowledge, single-crystal Pd nanowires as plasmonic waveguides have not yet been demonstrated, which is mainly due to the difficulties in having efficient photon–plasmon coupling and the robust plasmon propagating in Pd single nanowires, including: (1) the large dispersion mismatch between the wave vectors of photons and surface plasmon polaritons (SPPs) usually induces low photon–plasmon coupling efficiency;[25,26]

Dr. F. Gu, Prof. H. Zeng, Prof. S. Zhuang
Shanghai Key Laboratory of Modern Optical System
School of Optical-Electrical and Computer Engineering
University of Shanghai for Science and Technology
Shanghai, 200093, China
E-mail: hpzeng@phy.ecnu.edu.cn
Dr. Y. B. Zhu, Prof. L. K. Ang
Engineering Product Development
Singapore University of Technology and Design
Singapore, 138682, Singapore
Prof. Q. Yang
State Key Laboratory of Modern Optical Instrumentation
Department of Optical Engineering
Zhejiang University
Hangzhou, 310027, China

DOI: 10.1002/adom.201300413

(2) the large intrinsic losses at optical frequency of Pd material shorten the plasmon propagation length and thus limit the practicality of single-crystal Pd nanowires.[27,28]

In this work for the first time, we demonstrated efficient excitation and propagation of surface plasmon in single-crystal Pd nanowires. Based on an evanescent wave coupling technique, light is efficiently coupled into the Pd single nanowires using optical fiber tapers. The plasmon propagation losses of Pd nanowires on an MgF_2 substrate at the wavelength of 635 nm were measured to be ~2 dB/μm. Using a suspension scheme of the nanowire, the propagation losses decreased to ~0.6 dB/μm in air surrounding. Via alloying technique, silver was used as a gain medium to fabricated single-crystal PdAg nanowires and exhibited decreasing and tunable propagation losses. Finally, single-crystal Pd nanowires were used for plasmonic gas sensing with amplitude sensitivity of ~11 dB to 3.6% hydrogen gas and a concentration detection limit down to 0.2%.

2. Plasmon Propagation in MgF_2-supported Pd Nanowires

The single-crystal Pd nanowires used were fabricated by a simple vapor transport method (see Experimental Section).[23,24] Vertical Pd nanowires were grown on a c-cut sapphire substrate at a source temperature of 1250 °C, with lengths ranging from several micrometers to tens of micrometers (Figure S1, Supporting Information). As-fabricated Pd nanowires showed smooth outer surface and excellent cross-section uniformity without obvious structural defects. For example, **Figure 1**a shows a low-resolution transmission electron microscope (TEM) image of a typical 100 nm diameter Pd nanowire. The excellent diameter uniformity and sidewall smoothness make the nanowire suitable for low-loss plasmonic propagating. The high-resolution TEM image in Figure 1b and its corresponding selected area electron diffraction (SAED) pattern confirm that as-fabricated Pd nanowires were single crystalline without twins or defects and grow along the [110] direction.

As-fabricated Pd nanowires were removed from the original as-grown sample and dispersed onto an MgF_2 substrate (refractive index ~1.39). To excite SPPs, we used a silica optical fiber taper to couple light into the Pd single nanowires based on an evanescent wave coupling technique, which has been proved highly efficient and compact for coupling light into nanoscale waveguides such as silica nanofibers,[29] semiconductor nanowires[17,30] and polymer nanowires.[21,31] As illustrated in Figure 1c, excitation light from a standard silica optical fiber was first squeezed into a fiber taper with tip diameter in the range of 100~500 nm (see Experimental Section and Figure S2); then the evanescent wave outside the fiber taper was scattered at the distal end of the fiber taper with a broad distribution of wave vectors (k_{SPP}), in order to match the momentum of photons and plasmons.[26,32,33] By placing the fiber taper and the nanowire in parallel and close contact within a few micrometers, optical near-fields in the fiber taper and the nanowire will strongly overlap, resulting in highly efficient coupling of photons and plasmons. Figure 1d shows optical micrographs of 635- and 808-nm wavelength monochromatic lasers and a broadband supercontinuum (SC) source coupled into a 290 nm diameter

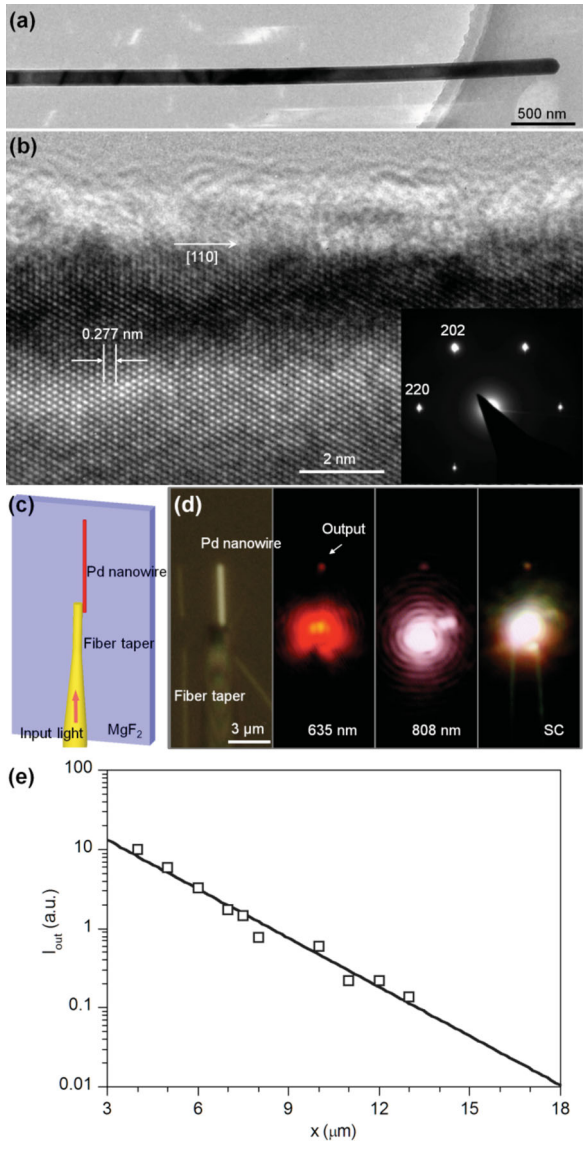

Figure 1. (a) TEM image of a typical 100-nm diameter Pd nanowire. (b) High-resolution TEM image of the Pd nanowire. Inset shows its corresponding SAED pattern. (c) Schematic diagram of the excitation of SPPs in an MgF_2-supported Pd nanowire using a fiber taper. (d) Optical micrographs of an MgF_2-supported 290-nm diameter Pd nanowire coupled with a silica fiber taper and its guiding 635-, 808-nm light, and a broadband SC source, respectively. (e) Propagation distance-dependent output intensity of a 200-nm diameter Pd nanowire at 635-nm wavelength.

Pd nanowire, respectively. After propagating with a distance of about 6 μm, light emitted at the distal end of the nanowire with no scattered spots observed at the body of the nanowire. Even with weak signals, the output spots could be easily distinguishable from surrounding environments. These results suggested the effective excitation and propagation of SPPs in the Pd nanowire.

The propagation losses (α) of the Pd single nanowires on the MgF_2 substrate were investigated by placing a light-coupling fiber taper at different locations along the Pd nanowire and measuring the corresponding output light intensity (I_{out}) at the

output end of the nanowire.[34,35] Figure 1e plots the measured I_{out} at the wavelength of 635 nm against varying propagation distances (x) in a 200 nm diameter Pd nanowire. These data could be well-fitted by a first-order exponential decay function $I_{out}/I_0 = \exp(-\alpha x)$, where I_0 is the normalized input intensity and α is the propagation loss. The obtained propagation loss at the wavelength of 635 nm was about 1.93 dB/μm, corresponding to a propagation length (L, $1/e$ damping intensity of the SPPs) of 2.5 μm. The propagation losses were also carried out in several other Pd nanowires with different diameters and α was from 2.3 to 1.9 dB/μm, which was much larger than that of Ag nanowires (e.g., 0.41 dB/μm at 633 nm wavelength)[34] as expected.

To understand the behavior of the plasmon propagation, we characterized the cross-section of the Pd nanowires. The top-view scanning electron microscope (SEM) image of the Pd nanowires in **Figure 2**a and a typical cross-sectional SEM image (cut by a focused ion beam) of a Pd nanowire in Figure 2b show that the cross-sections of the Pd nanowires were in triangle shape. Using COMSOL Multiphysics, we simulated the energy density distribution in the Pd nanowire waveguides. Figures 2c–e show the energy density distributions of three lowest order modes of SPPs at the cross section of an MgF_2-supported 200 nm diameter Pd nanowire excited by 635 nm wavelength light. The simulations clearly show that these SPP modes are hybridized modes (denoted H_0, H_1, and H_2) due to the substrate mediating effect,[36] and the energy are highly concentrated at the triangle tips. The corresponding calculated propagation losses are about 10.12, 3.98, and 0.72 dB/μm for the H_0, H_1, and H_2 modes, respectively. These values suggest that our measured losses were the likely to be a weighted average of all the propagation modes in the Pd nanowires.

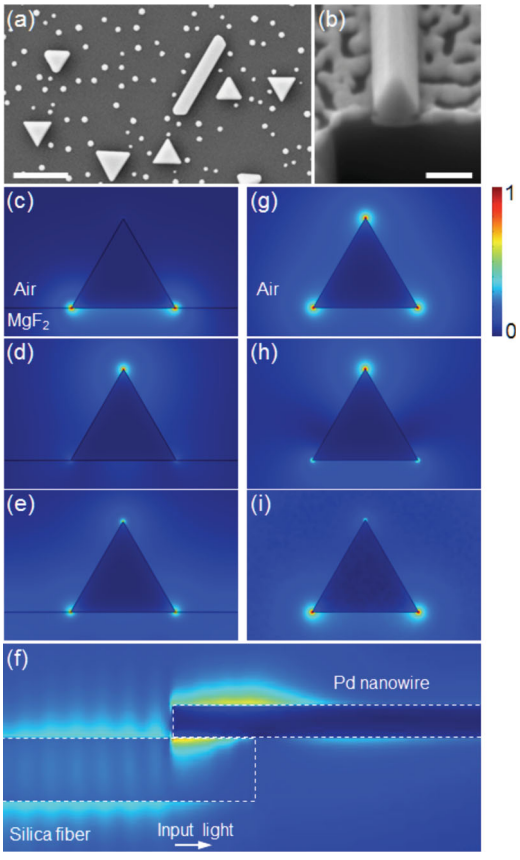

Figure 2. (a) Top-view SEM image of the Pd nanowires. Scale bar: 500 nm. (b) Typical cross-sectional SEM image (cut by a focused ion beam) of the Pd nanowire. Scale bar: 100 nm. (c–e) Energy density distribution at the cross section of a MgF_2-supported 200 nm diameter Pd nanowire for the modes of H_0, H_1, and H_2, respectively. The wavelength of excitation light is 635 nm. (f) Simulation of coupling between a 200-nm diameter silica fiber and a 100-nm diameter Pd nanowire at air cladding condition, with an overlap of 1 μm. (g–i) Energy density distribution at the cross section of a 100 nm diameter Pd nanowire at air cladding condition for the modes of fundamental mode and two high-order modes, respectively.

3. Plasmon Propagation in Suspended Pd Nanowires

For waveguides used in plasmonic devices and systems, such short propagation lengths are insufficient to build a robust circuit that contains several components, and alternative approaches are needed to adapt the Pd nanowires for long-distance plasmon propagating. As it has been successfully demonstrated in polymer and semiconductor nanowires,[17,31] using the suspension approach to enable low-loss and broadband waveguiding could also be applicable to Pd nanowires for long-distance plasmon propagating. As illustrated in **Figure 3**a, a Pd nanowire was supported by the tip of a suspended fiber taper in air (see Experimental Section and Figure S3). Figure 3b shows the optical micrographs of an 85 nm diameter Pd nanowire supported by a fiber taper in air, and its guiding lasers at different wavelengths of 635 and 808 nm and a SC source, respectively. Notable bright light spots were observed at the distal end of the nanowire with a propagating distance about 11 μm. Much longer SPP propagation distances were also observed in other Pd nanowires (e.g., over 30 μm, Figure S4). The long SPP propagation distances make it easy to collect the output light with low background noise, which is very important for sensing application. The spectrum at the distal end of the 85 nm diameter Pd nanowire guiding a SC source is shown in Figure 3c, from which a broad transmittability of the Pd nanowire in the visible and near infrared spectral range is clearly seen.

Figure 3d shows a typical propagation loss of about 0.61 dB/μm at 635 nm wavelength in a 150 nm diameter Pd nanowire (in air surrounding), corresponding to a propagation length of 7.1 μm. The results carried out in several other Pd nanowires were observed to range from 0.5 to 0.7 dB/μm. Simulation in Figure 2f shows that with an overlap of 1 μm between a 200-nm diameter silica fiber and a 100-nm diameter Pd nanowire, more than 20% of the 635-nm light energy (fundamental mode) could be transferred from the silica fiber to the Pd nanowire. However, the fundamental mode (m = 0) of the SPPs experienced a large damping in a distance of ~2 μm, and then only the high-order mode (e.g., m = ± 1, ± 2) could be stably guided. Figures 2g–i show the energy density distributions of a 100 nm diameter Pd nanowire for the fundamental mode and two typical high-order modes (m = 1 and 2) at 635 nm wavelength, respectively, with the calculated propagation losses of 7.42, 2.56, and 0.26 dB/μm, respectively. These

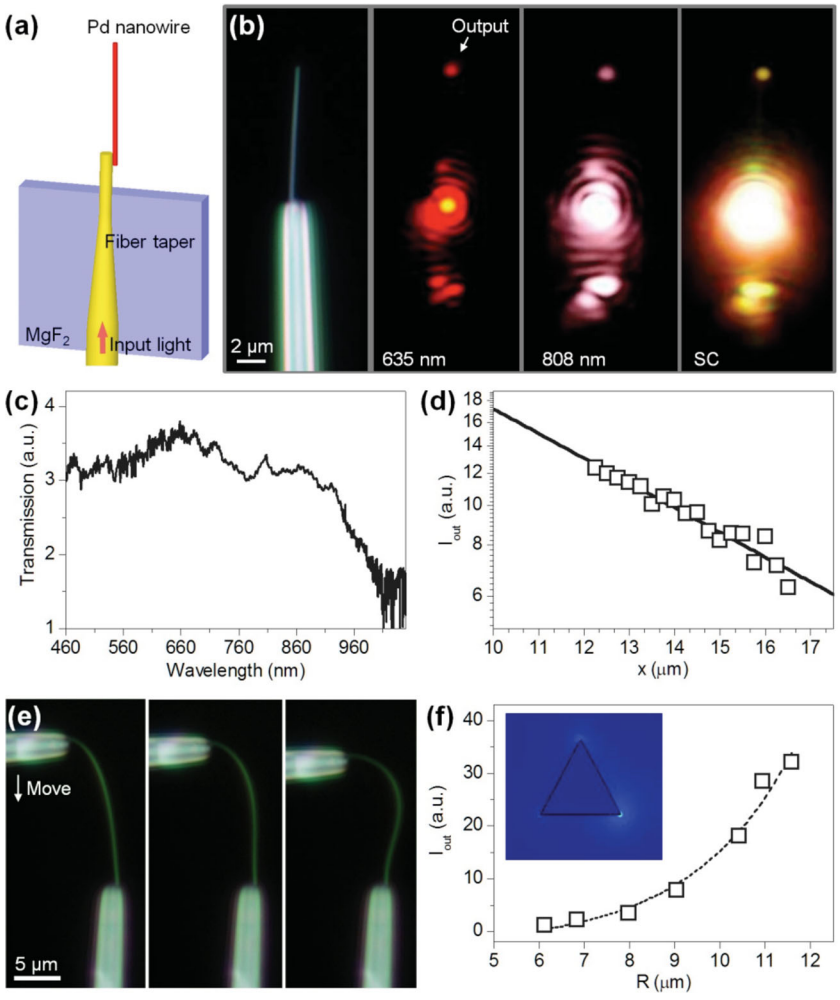

Figure 3. (a) Schematic diagram of a Pd nanowire with one end coupled with a suspended fiber taper. The fiber taper was supported on a MgF_2 substrate. (b) Optical micrographs of a 85-nm diameter Pd nanowire coupled with a silica fiber taper and its guiding 635-, 808-nm light, and a broadband SC source, respectively. (c) Transmission spectrum of the 85-nm diameter Pd nanowire. (d) Propagation distance-dependent output intensity of a 150-nm diameter Pd nanowire at 635-nm wavelength. (e) Optical micrographs of bending a Pd nanowire by moving one fiber taper. (f) Bending radius-dependent output intensity of a 130-nm diameter Pd nanowire at 635-nm wavelength. Inset shows the energy density of the fundamental mode in the 130 nm diameter Pd nanowire with an 8 μm bending radius.

values also suggest that the losses obtained here were mainly contributed from all the higher-order propagation modes. Compared with the lower-order modes, the higher-order SPP modes show less propagation losses and longer propagation ranges. In metal nanowires the propagation losses in the visible and ultra-violet spectral ranges mainly arise from the intrinsic ohmic loss. The higher-order modes confine a lower fraction of the SPP energy within the metal nanowires compared to the lower-order modes, and thus induce less propagation losses.[12–14]

As curved waveguides are important building blocks in integrated devices such as couplers, resonators and interferometers,[35,37] the bending properties of plasmonic propagating in the Pd nanowires were preliminarily investigated by using two mutually perpendicular suspended fiber tapers (see Figure 2e and Experimental Section). Figure 2f shows that in a Pd nanowire with a diameter of 130 nm and a length of 16 μm, when the bending radius (R) changed from 12 μm to 6 μm, the intensity of I_{out} decreased over 90%, which provided helpful knowledge for designing bent Pd nanowire-based plasmonic devices. The bending loss occurs because bending changed the momentum of k_{SPP} and induced light radiation.[35] The simulation in the inset of Figure 3f also shows that in the 130 nm diameter Pd nanowire with an 8 μm bending radius, the energy density of the fundamental mode degenerated from symmetrically distribution around three triangle tips (see reference in Figure 2g) to only one tip. Compared with other plasmonic and photonic nanowires,[35,37] the bending losses are larger in the Pd nanowires. In our approach, the total losses of the measured I_{out} in a curved Pd nanowire were the combination of the propagation loss and pure bending loss, and were affected by other experimental parameters such as bending angle and the diameters of the nanowire, which needs further study in the future.

4. Plasmon Propagation in PdAg Alloy Nanowires

Via alloy technique by introducing other metal materials, the propagation loss of the Pd nanowires could be tuned.[23,28,38] Silver material has lowest loss in visible spectrum and here it was used to fabricate PdAg alloy nanowires. Using the same vapor transport method (see Experimental Section), a continuous spatial composition grading was attained for single-crystal Pd_xAg_{1-x} ($0< x <1$) alloy nanowires fabricated on a sapphire substrate. **Figure 4**a shows a high-resolution TEM image and its SAED pattern of a representative as-fabricated PdAg nanowire, indicating the structure of single-crystal metallic compound. The in-situ energy dispersive spectrometry (EDS) shown in Figure 4b reveals the composition ratio of [Pd]/[Ag] to be 0.67/0.33. The red line in Figure 4c plots the propagation distances-dependent I_{out} of a 240-nm diameter $Pd_{0.81}Ag_{0.19}$ nanowire supported on the MgF_2 substrate, where a propagation loss of 1.8 dB/μm was obtained. By increasing the Ag proportion, the loss could be further decreased. In a 210-nm diameter $Pd_{0.45}Ag_{0.55}$ nanowire, a measured propagation loss of 1.2 dB/μm was obtained, as shown in the blue line. As a reference, Figure 4d shows the optical micrographs of the $Pd_{0.45}Ag_{0.55}$ nanowire guiding light at 635 and 808 nm and a SC source, respectively. Clear light spots were observed at the distal end of the nanowire with a propagating distance of about 10 μm.

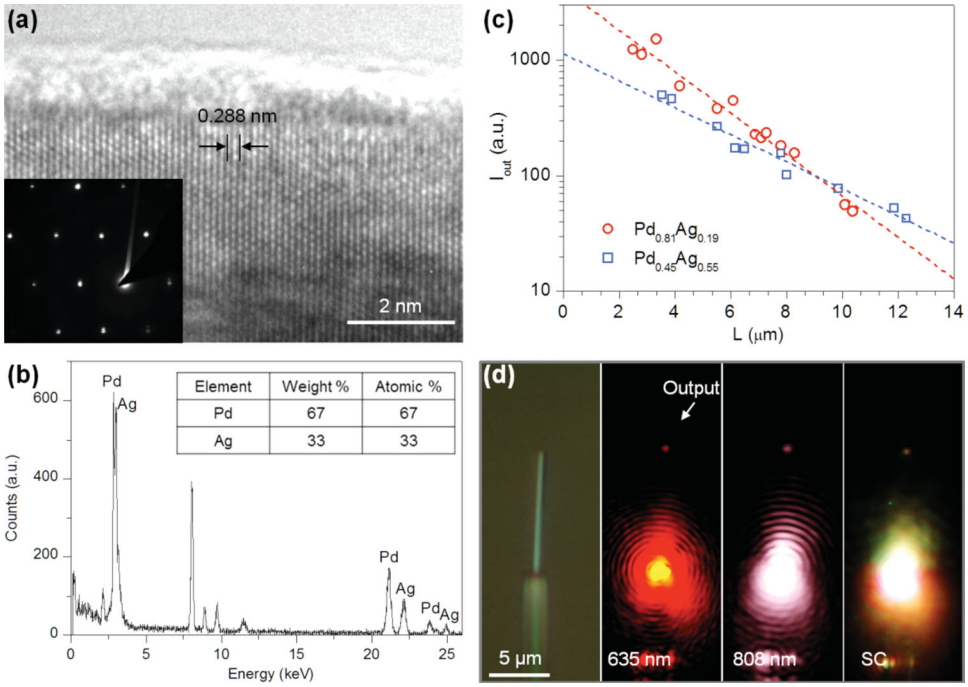

Figure 4. (a) High-resolution TEM image of a PdAg nanowire. Inset shows its corresponding SAED pattern. (b) In situ EDS of the nanowire. (c) Propagation distance-dependent output intensity at 635-nm wavelength obtained in a 240-nm diameter $Pd_{0.81}Ag_{0.19}$ nanowire and a 210-nm diameter $Pd_{0.45}Ag_{0.55}$ nanowire. (d) Optical micrographs of the 210-nm diameter $Pd_{0.45}Ag_{0.55}$ nanowire coupled with a silica fiber taper and its guiding 635-, 808-nm light, and a SC source, respectively.

5. Highly Sensitive Hydrogen Detection

As shown in **Figure 5**a–c, a Pd nanowire was coupled using two suspended fiber tapers for light launching and collection. The Pd nanowire and the two fiber tapers were sealed inside a plastic chamber with a gas inlet/outlet (Figure 5d).[31,32] The detection light used was a continuous-wave monochromatic laser with a wavelength of 980 nm. The red line in Figure 5e plots the light transmission change in logarithmic scale of a Pd nanowire with a diameter of 92 nm and a length of 15 μm, as hydrogen concentration increased from 0 to 6.5%. It was found that at low hydrogen concentration (<2%) the light transmission decreased slowly with a change of ~0.7 dB; and then as hydrogen concentration increased from 2.5% to 3.6% the light transmission decreased rapidly with a change of ~10.4 dB. As hydrogen concentration increased higher than 4%, the light transmission increased slowly and showed saturation. For hydrogen concentration from 0% to 3.6%, the transmission shows monotonous decrease with a change of ~11 dB (92%). Compared with the transmission change in hydrogen sensors based on photonic nanowires reported so far,[19,39] the Pd nanowire shows lower amplitude sensitivity at low hydrogen concentration; however, the transmission change of over 11 dB in Pd nanowires to 3.6% hydrogen is much higher than those of less than 3 dB (50%) in photonic nanowire sensors. The obtained high amplitude sensitivity shows the potential to develop high-sensitive Pd-nanowire based plasmonic sensing devices. The detection limit of hydrogen concentration is about 0.2%, which is lower than those in photonic nanowire sensors and most of surface plasmon resonance hydrogen sensors reported so far.[40–42]

It is known that the response of the Pd-H system follows the "pressure-composition" isotherms as illustrated in the inset of Figure 5e.[3,6] The observed non-monotonous light transmission variation with hydrogen concentration could be understood as follows: (1) At low concentration, hydrogen molecules absorbed on the nanowire surface, diffused into the nanowire lattices, and then formed an interstitial dilute solid solution (α-phase). In this process, surface scattering of electrons dominated the transmission loss. (2) As concentration further increased, a palladium hydride phase (β-phase) gradually formed and weakened the optical absorption at the 980-nm detection wavelength. Thus in the coexistence region of α- and β-phase, whether the transmission decrease or increase was dependent on the competition between the electron scattering and the optical absorption of the β-phase. In our case, the electron surface scattering[9] dominated the transmission loss in the coexistence region. The competition process could also be found in the dynamic process of the Pd nanowire to hydrogen gas. The typical time responses of the nanowire in the α-, β-phase, and their coexistence region are shown in Figures 5f, g, and h, respectively. Compared with the none or small fluctuation in the α- and β-phase single states, the response curve of the coexistence phase state fluctuated strongly, indicating the complicated and intense dynamic process between the two phase states. It could be attributed to the high single crystalline structure quality that allows Pd lattices to interact with hydrogen atoms more collectively than that in amorphous Pd nanostructures.[43] To our knowledge, such strong fluctuation in dynamic responses has not yet been reported in other polycrystalline Pd nanostructures.

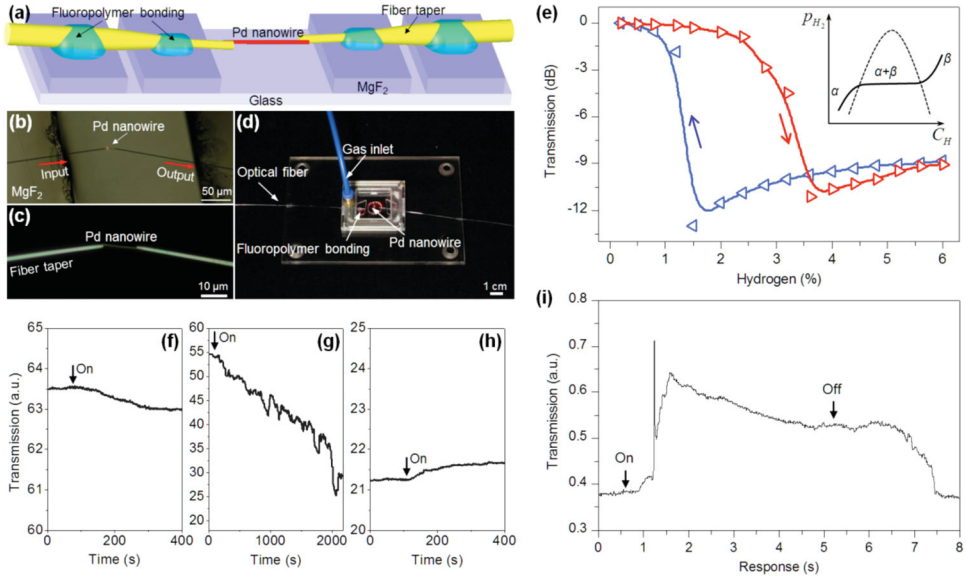

Figure 5. (a) Schematic diagram and (b–d) optical micrographs of a Pd nanowire coupled with a silica fiber taper and its guiding 635-nm light. For robust gas sensing, the fiber tapers were firmly bound on MgF_2 substrate using low-index UV-cured fluoropolymer. (e) Transmissions at 980 nm detection wavelength of a Pd nanowire with a diameter of 92 nm and a length of 15 μm as the hydrogen concentration increased (red line) and decreased (blue line). Inset illustrates the "pressure-composition" isotherms of the Pd-H system. Time responses of the nanowire as the hydrogen concentrations changed from (f) 0.2% to 0.5%, (g) 3.2% to 3.6%, and (h) 5.2% to 6%. (i) Typical response of a single-crystal $Pd_{0.84}Au_{0.16}$ alloy nanowire to 6% hydrogen at 635 nm detection wavelength.

The desorption process of hydrogen from the Pd nanowire was also investigated by decreasing hydrogen concentration from 6.5% to 0. As plotted in the blue line in Figure 5e, a similar (but reversed) qualitative behavior was found; however, the response curve did not return to the original position in the hydrogen adsorption process, indicating a strong hysteresis effect of the Pd nanowire for hydrogen detection. The transmission strongly changed at concentration from 1.5% to 0.8%, which was smaller than that as hydrogen concentration increased (from 2.4% to 3.6%). The reversible response of a Pd nanowire by cycling 0–10% hydrogen is provided in Figure S5 (Supporting Information), in which good reversibility of the Pd nanowire is clearly seen.

The hysteresis effect arises from the lattice strain resulting from hydrogen and/or residual hydrogen atoms that cannot be desorbed from the Pd nanowire at room temperature.[10,11] To develop single-crystal Pd nanowire for future practical hydrogen sensing application the hysteresis effect is the major challenge, because this effect can cause some harmful sensor behavior, such as slow response and long recovery time. By doping with other metals such as Ni or Au, this effect could be decreased or avoided.[44] For example, Figure 5i shows a typical response of a single-crystal $Pd_{0.84}Au_{0.16}$ alloy nanowire to 6% hydrogen at 635 nm detection wavelength, in which the transmission returned to its original position quickly when the hydrogen gas was turned off. Compared with those of the pure Pd nanowires the response time (~0.5 s) and the recovery time (~2 s) of the $Pd_{0.84}Au_{0.16}$ alloy nanowire were also improved. In addition, using alloy nanowires such as PdAu and PdAg can also decrease the propagation loss and has the possibility to develop resonant sensing structures with high sensitivity and resolution.[45]

6. Conclusion

Based on an evanescent wave coupling technique using optical fiber tapers, we have demonstrated efficiently excitation and propagation of SPPs in single-crystal Pd nanowires in 2 different conditions of substrate supporting and air surrounding. The large intrinsic losses of Pd nanowires are demonstrated decreasing and tunable via alloying technique. The responses of the Pd nanowires to hydrogen gas were further investigated with amplitude sensitivity as high as 11 dB to 3.6% hydrogen and a concentration detection limit down to 0.2%, which is benefited from the sub-wavelength tight surface confinement of SPPs and the enhanced interaction of light with the Pd nanowire waveguides. The hysteresis effect of the Pd nanowire for hydrogen sensing was investigated and the single-crystal PdAu alloy nanowires were adopted to suppress this effect. Since the fiber taper enabled efficient connection with outer standard optical fiber systems, the single-crystal Pd and its alloy nanowire waveguides may find promising applications in compact plasmonic sensing devices. More generally, our results can also be applied to other single-crystal metal nanowires besides the conventional Au and Ag nanowires used for plasmon propagation applications, and will stimulate the synthesis of new functional single-crystal element and alloy nanowire waveguides. We believe that this will open up vast opportunities in nanophotonic and nanoplasmonic areas.

7. Experimental Section

Fabrication of Pd Nanowires and its Alloy Nanowires: The single-crystal Pd nanowires used were fabricated in a horizontal alumina tube mounted inside a single-zone furnace (GSL-1600X, Hefei Kejing

Materials Technology Co., Ltd.). In the tube (inter diameter 60 mm, length 120 cm) an alumina boat with 0.1 g Pd powder (Sinopharm Chemical Reagent Co., Ltd., SCRC, 99.99% purity) was placed in the center of the heating zone. Several pieces of c-cut single crystal sapphire substrates (5 mm × 5 mm) were placed downstream of the gas flow and separately about 8 cm from the center. Prior to heating, high-purity Ar gas was introduced into the quartz tube at a flow rate of 800 sccm to purge air from the tube. After 30 min, the furnace was rapidly heated to 1250 °C in 35 min and the pressure was maintained at 300 mbar. After 1 h of growth at 1250 °C, the temperature was reduced to room temperature. Vertical Pd nanowires with lengths ranging from several micrometers to tens of micrometers were grown on the sapphire substrate.

Single-crystal PdAg and PdAu alloy nanowires were prepared through the same procedure. For the PdAu alloy nanowires, the evaporation source was a mixture of 0.1-g Pd powder and 0.5-g Ag powder (SCRC, 99.9% purity) with a evaporation temperature of 1200 °C, and for the PdAu alloy nanowires the evaporation source was a mixture of 0.1-g Pd powder and 0.3-g Au powder (SCRC, 99.9% purity) with a evaporation temperature of 1250 °C. Single-crystal Pd_xAg_{1-x} and Pd_xAu_{1-x} ($0 < x < 1$) alloy nanowires of continuous spatial composition grading were fabricated along the length direction of the sapphire substrates.

Investigation of Plasmon Propagation and Hydrogen Detection: As-fabricated Pd and its alloy nanowires were first removed from the growth substrates onto an MgF_2 substrate by mechanical scratching. To efficiently excite the plasmon propagation in Pd and its alloy single nanowires, we used an evanescent wave coupling technique. In our approach, excitation light was first lens-coupled into a standard silica fiber (SMF-28, Corning) and then squeezed into a fiber taper with tip diameter in the range of 100~500 nm. The fiber tapers were drawn from the standard optical fiber by using a simple flame-heated method. Then, under an optical microscope (Nikon 80i) equipped with superlong-working distance objectives, the fiber taper mounted on a triple-axis micromanipulator (M-462, Newport) was precisely connected to the Pd nanowires via evanescent wave coupling (see Figure S2).

To investigate the plasmon propagation property in air surrounding condition, a fiber taper was first bound to an MgF_2 substrate using a low-index UV cured fluoropolymer,[21,31,32] and the tip of the fiber taper protruded out of the substrate with a distance of ~50 μm; then the Pd and its alloy nanowires were picked up from the growth substrates by a fiber taper with a sharp tip via micromanipulation and placed parallelly at the tip of the suspended silica fiber taper in air (see Figure S3).

To investigate the responses of Pd its alloy nanowires to hydrogen gas, the nanowires and the two fiber tapers were all sealed inside a plastic chamber with a gas inlet/outlet.[31,32] The hydrogen gas diluted with Ar gas was introduced into the chamber at a flow rate of about 100 sccm while the transmittance of the nanowire was measured with continuous-wave monochromatic lasers. All experiments are carried out at room temperature and atmospheric pressure.

The excitation light sources with wavelengths of 635, 808, and 980 nm were continuous-wave monochromatic lasers, and the broadband light was from a SC source (SuperK Compact, NKT photonics). The output from the nanowires was collected using long-working-distance microscope objectives and directed to spectrometers (QE65 Pro, Ocean Optics; and AQ6370C, Yokogawa) and a CCD camera, respectively.

Supporting Information

Supporting Information is available from the Wiley Online Library or from the author.

Acknowledgements

This work was partly supported by the National Natural Science Foundation of China (11304202, 10990101 and 91221304), National Key Scientific Instrument Project (2012YQ150092), and National Basic Research Program of China (2011CB808105).

Received: October 7, 2013
Revised: November 24, 2013
Published online: December 12, 2013

[1] M. E. Stewart, C. R. Anderton, L. B. Thompson, J. Maria, S. K. Gray, J. A. Rogers, R. G. Nuzzo, *Chem. Rev.* **2008**, *108*, 494.
[2] J. Tsuji, *Palladium Reagents and Catalysts: New Perspectives for the 21st Century*, 2nd ed., Wiley, Chichester, England **2004**.
[3] T. B. Flanagan, W. A. Oates, *Annu. Rev. Mater. Sci.* **1991**, *21*, 269.
[4] T. Hübert, L. Boon-Brett, G. Black, U. Banach, *Sens. Actuat. B* **2011**, *157*, 329.
[5] Y. Xiong, B. Wiley, J. Chen, Z.-Y. Li, Y. Yin, Y. Xia, *Angew. Chem. Int. Ed.* **2005**, *44*, 7913.
[6] C. Langhammer, I. Zorić, B. Kasemo, *Nano Lett.* **2007**, *7*, 3122.
[7] C. Xiao, H. Ding, C. Shen, T. Yang, C. Hui, H.-J. Gao, *J. Phys. Chem. C* **2009**, *113*, 13466.
[8] F. Favier, E. C. Walter, M. P. Zach, T. Benter, R. M. Penner, *Science* **2001**, *293*, 2227.
[9] F. Yang, K. C. Donavan, S.-C. Kung, R. M. Penner, *Nano Lett.* **2012**, *12*, 2924.
[10] I. Zorić, E. M. Larsson, B. Kasemo, C. Langhammer, *Adv. Mater.* **2010**, *22*, 4628.
[11] N. Liu, M. L. Tang, M. Hentschel, H. Giessen, A. P. Alivisatos, *Nat. Mater.* **2011**, *10*, 631.
[12] T. W. Ebbesen, C. Genet, S. I. Bozhevolnyi, *Phys. Today* **2008**, *61*, 44.
[13] S. Lal, S. Link, N. J. Halas, *Nat. Photon* **2007**, *1*, 641.
[14] H. Wei, H. X. Xu, *Nanophoton.* **2012**, *1*, 155.
[15] A. Tittl, P. Mai, R. Taubert, D. Dregely, N. Liu, H. Giessen, *Nano Lett.* **2011**, *11*, 4366.
[16] T. Kang, W. Choi, I. Yoon, H. Lee, M.-K. Seo, Q.-H. Park, B. Kim, *Nano Lett.* **2012**, *12*, 2331.
[17] F. Gu, L. Zhang, H. Yu, W. Fang, J. Bao, L. Tong, *Nanotechnol.* **2011**, *22*, 425201.
[18] P. Wang, L. Zhang, Y. Xia, L. Tong, X. Xu, Y. Ying, *Nano Lett.* **2012**, *12*, 3145.
[19] D. J. Sirbuly, S. E. Letant, T. V. Ratto, *Adv. Mater.* **2008**, *20*, 4724.
[20] Q. Yang, X. Jiang, X. Guo, Y. Chen, L. Tong, *Appl. Phys. Lett.* **2009**, *94*, 101108.
[21] F. Gu, H. Yu, P. Wang, Z. Yang, L. Tong, *ACS Nano* **2010**, *4*, 5332.
[22] M. A. Foster, A. C. Turner, M. Lipson, A. L. Gaeta, *Opt. Express* **2008**, *16*, 1300.
[23] Y. Yoo, K. Seo, S. Han, K. S. K. Varadwaj, H. Y. Kim, J. H. Ryu, H. M. Lee, J. P. Ahn, H. Ihee, B. Kim, *Nano Lett.* **2010**, *10*, 432.
[24] Y. Yoo, I. Yoon, H. Lee, J. Ahn, J.-P. Ahn, B. Kim, *ACS Nano* **2010**, *4*, 2919.
[25] J. M. Pitarke, V. M. Silkin, E. V. Chulkov, P. M. Echenique, *Rep. Prog. Phys.* **2007**, *70*, 1.
[26] R. X. Yan, P. Pausauskie, J. X. Huang, P. D. Yang, *Proc. Natl. Acad. Sci. USA* **2009**, *106*, 21045.
[27] E. D. Palik, *Handbook of Optical Constants of Solids* Academic Press, Boston **1991**.
[28] P. R. West, S. Ishii, G. V. Naik, N. K. Emani, V. M. Shalaev, A. Boltasseva, *Laser Photonics Rev.* **2010**, *4*, 795.
[29] L. Tong, R. R. Gattass, J. B. Ashcom, S. He, J. Lou, M. Shen, I. Maxwell, E. Mazur, *Nature* **2003**, *426*, 816.
[30] M. Law, D. J. Sirbuly, J. C. Johnson, J. Goldberger, R. J. Saykally, P. Yang, *Science* **2004**, *305*, 1269.
[31] F. Gu, L. Zhang, X. Yin, L. Tong, *Nano Lett.* **2008**, *8*, 2757.
[32] F. Gu, H. Zeng, L. Tong, S. Zhuang, *Opt. Lett.* **2013**, *38*, 1826.

[33] X. Guo, M. Qiu, J. M. Bao, B. J. Wiley, Q. Yang, X. Zhang, Y. G. Ma, H. K. Yu, L. M. Tong, *Nano Lett.* **2009**, *9*, 4515.
[34] Y. G. Ma, X. Y. Li, H. K. Yu, L. M. Tong, X. Gu, Q. H. Gong, *Opt. Lett.* **2010**, *35*, 1160.
[35] W. Wang, Q. Yang, F. Fan, H. Xu, Z. L. Wang, *Nano Lett.* **2011**, *11*, 1603.
[36] S. Zhang, H. Xu, *ACS Nano* **2012**, *6*, 8128.
[37] H. Yu, S. Wang, J. Fu, M. Qiu, Y. Li, F. Gu, L. Tong, *Appl. Opt.* **2009**, *48*, 4365.
[38] M. G. Blaber, M. D. Arnold, M. J. Ford, *J. Phys.: Condens. Matter* **2010**, *22*, 143201.
[39] J. Villatoro, D. Monzón-Hernández, *Opt. Express* **2005**, *13*, 5087.
[40] B. Chadwick, J. Tann, M. Brungs, M. Gal, *Sens. Actuat. B* **1994**, *17*, 215.
[41] A. Tittl, P. Mai, R. Taubert, D. Dregely, N. Liu, H. Giessen, *Nano Lett.* **2011**, *11*, 4366.
[42] X. Bévenot, A. Trouillet, C. Veillas, H. Gagnaire, M. Célmen, *Meas. Sci. Technol.* **2002**, *13*, 118.
[43] F. Gu, H. Yu, W. Fang, L. Tong, *Opt. Express* **2012**, *20*, 8667.
[44] Z. Zhao, Y. Sevryugina, M. A. Carpenter, D. Welch, H. Xia, *Anal. Chem.* **2004**, *76*, 6321.
[45] F. Xu, P. Horak, G. Brambilla, *Opt. Express* **2007**, *15*, 7888.